2026 IEEE International Conference on Robotics and Automation (ICRA 2026)
June 1-5, 2026. Vienna, Austria

Hydrodynamic Optimization of a Spherical Amphibious Robot's Paddle-Wheel for Effective Water Surface Locomotion*

Muhammad Affan Arif[#], Jiyuan Song[#*], Yao Tu[*], Yihui Duan, Shuangge Yang and Qingquan Li

***Abstract*—This paper presents the design, dynamic modeling, and hydrodynamic optimization of an amphibious hybrid differential-drive spherical robot capable of operating on both land and water. The robot adopts a three-module symmetric structure, where dual paddle-wheel actuators enable forward motion, in-place turning, and arc-turning maneuvers. To address pitch oscillations during operation, a hierarchical cascade controller with current, velocity, and attitude compensation loops is implemented, ensuring stable performance across different environments. Four paddle-wheel designs based on helical screw-thread geometry were systematically analyzed through computational fluid dynamics (CFD) simulations. The Helix-2 configuration exhibited the best balance between thrust and lateral force generation. Experimental validation on a custom-built test-bed confirmed these findings: compared with straight-blade paddles, Helix-2 achieved up to 51% improvement in forward thrust and a maximum lateral force improvement exceeding 160%. The results demonstrate that the proposed spherical robot achieves energy-efficient amphibious locomotion with improved maneuverability, making it suitable for inspection, monitoring, and tasks in confined water–land transition environments.**

***Index Terms*—Mobile robot, spherical robot, amphibious robot, and hydrodynamic optimization.**

I. Introduction

Spherical robots, on one hand due to their spherical shape, promise exceptional mobility that other types of mobile robots cannot offer [1]. Their primary mode of motion is rolling, which is more efficient than other modes of motion. These robots are also free from the challenges of turning over and tipping over that exist in other mobile robots. Moreover, all the electronic equipment of the spherical robots is preserved inside their outer spherical shell, making them suitable for hazardous environments. On the other hand, the spherical shape of these robots also brings forth their own unique challenges. Their outer spherical shell establishes a point contact with the ground, which makes it very easy to disturb their movement. Their shape also requires novel driving mechanisms as the traditional mechanisms cannot be used. Moreover, their non-holonomic motion further adds to the challenges of their dynamic modeling and motion control. Such problems have hindered the development of spherical robots and from realizing their true potential.

In an attempt to address the above mentioned problems, several researchers came up with novel designs of spherical robots. Pendulums have long been the most popular choice of the driving mechanism for the non-holonomic spherical robots. A single pendulum with two degrees of freedom is used to displace the center of mass of the spherical robot for straight and turning motion. However, the degrees of freedom of the pendulum enlarges the state space and limits the maximum length of the pendulum. In [2], a spherical robot with two coaxial pendulums with a single degree of freedom was presented, which turned using the inertial forces generate by the coaxial pendulums. The use of coaxial pendulums reduces the state space and increases the torque, but the precise control of the inertial force over different ground surfaces is a difficult task. Some designs with internal drive units have also been presented in the literature, in which a car or a ball is driven against the inner surface of the spherical shell to transmit torque via friction. However, the torque generated is limited, and the friction and slippage makes the control challenging. Recently, several designs are being presented that either use control moment gyroscopes or flywheels, or a combination of pendulums and flywheels[3]. Some promising results have been recently published by Zhejiang university with this propulsion strategy [4], [5]. However, the CMGs (Control Moment Gyroscopes) require constant rotation, which requires massive consistent power supply. Moreover, the precise control of the torque generated by the CMGs when combined with pendulums has its own challenges due to precession, and requires deep understanding of the dynamics of this mechanism, a diagnosis also pointed toward other spherical robot mechanisms[6]. Such mechanisms can benefit from thorough studies by isolating them from the spherical shell, as suggested previously. Besides these most common driving strategies, there are also some other designs presented in the literature, such as spherical shell shape deforming [7], [8], [9], displacement of internal masses [10], [11], and fluid displacement [12]. In paper [13] and [14], the combination displacement of masses and a single degree of freedom pendulum is presented for straight and arc-turning motion. However, for such design strategy, there must be a compromise between the pendulum length and the radius of curvature of the turning path of the robot.

Despite the strides made in the field of spherical robots, the existing designs still lack the mobility required for their deployment across various real-world practical applications, such as search and rescue operations during natural disasters, surveillance and monitoring of hazardous environments such as deep mines, pipes, and nuclear facilities, and extra-terrestrial space exploration. Up to date, only two

*This work was supported by Guangming Lab Funding under Grant 24410004. [#]Muhammad Affan Arif and Jiyuan Song are equal co-first authors. *([*]Corresponding author: Jiyuan Song and Yao Tu)*

Muhammad Affan Arif is with the Institute of Robotics & Intelligent Systems, Xi'an Jiaotong University, Xi'an, 710049, China (e-mail: affanarif025@hotmail.com).

Jiyuan Song, Yao Tu, Yihui Duan, Shuangge Yang and Qingquan Li are with the Guangdong Laboratory of Artificial Intelligence and Digital Economy (SZ), Shenzhen, 518107, China (e-mail: songjiyuan@gml.ac.cn; tuyao@gml.ac.cn; duanyihui@gml.ac.cn; 2643267626@qq.com; liqq@szu.edu.cn).

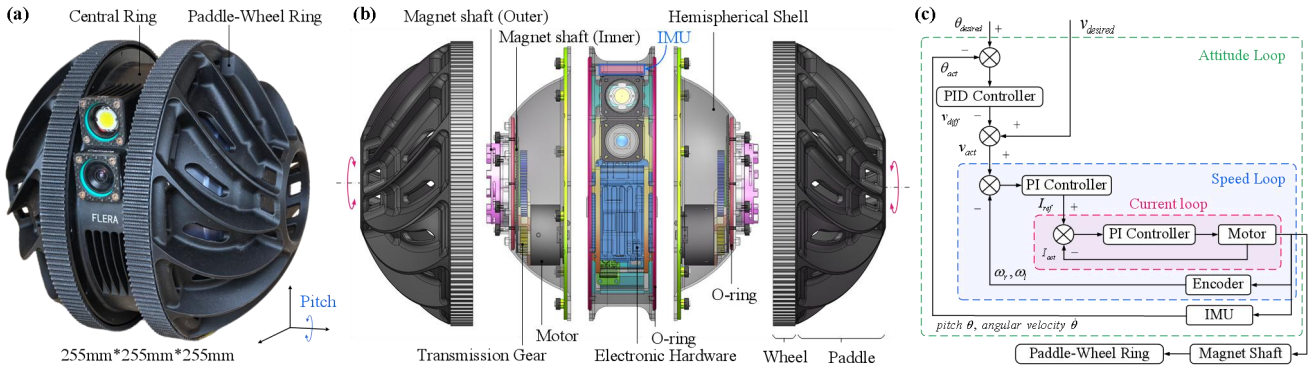

Fig. 1. Overview design of the spherical robot. (a) The spherical robot consists of a central ring module (which remains relatively stable during movement) and paddle-wheel ring modules symmetrically installed on the left and right sides (which can independently output rotational motion); (b) Detailed display of the proposed robot design. The central ring and the bilateral hemispherical side shells form a sealed cabin. Two motors are inside the cabin, outputting power via a gear-driven system and magnetic shaft coupling; (c) Control diagram of the robot. ω_r and ω_l deontes angular velocity of right and left wheels, respectively, and v denotes linear velocity of the robot.

spherical robots[4],[15] can be considered that were used for such real-world practical applications . An attempt was made at the monitoring application of the spherical robot in [16].

However, these robots also have not demonstrated capabilities suitable for a diverse set of applications. Especially the aquatic environment presents the biggest challenge for these robots. Very few spherical robots, such as [17], have been designed and studied for their swimming even though the sealed structure of the spherical robots makes them ideal for amphibious applications. Moreover, true versatility of these robots cannot be achieved without realizing agile and robust swimming capabilities.

In an attempt to address the above mentioned challenges, this paper uses an alternate approach to the design and presents a novel spherical robot that combines the advantages spherical robots and differential drive robots. Although some initial attempts were made to such designs in the early development history of the spherical robots, no extensive and successful studies have been reported in the literature. Although the designed spherical robot is intended for terrestrial and aquatic environments, since the swimming motion is the biggest challenge within the domain of spherical robot, this paper focuses on the design for aquatic environment. The main contribution of the paper are three folds:

1) A novel spherical robot is presented that combines the advantages of spherical robots and the differential drive robots. The result is a compact, light-weight, and agile spherical robot that can be deployed in both, in water and on land.

2) Inspired by paddle wheels, a novel propeller is designed, which compliments the unconventional shape of the spherical robots. This turns the shortcoming of these robots (no adequate space for extra mechanisms for swimming) into a strength (simplistic design for amphibious locomotion), ensuring high thrust force generation for agile aquatic motion, as validated through the robot's swimming experiments.

3) Multiphase turbulent computational fluid dynamics (CFD) simulations are performed for the optimization of the optimization of the design parameters of the paddle wheel based its hydrodynamic performance during its free surface motion. Such simulations have neither been reported in robotics nor propeller design literature to the best of authors' knowledge.

II. Methods

Although this paper focuses on the design and optimization for agile aquatic motion of the spherical robot, the designed robot can also move on land. The intention of the design was to combine the simplistic dynamics of differential drive robots with the unique structural advantages of the spherical robots. The result is an agile amphibious hybrid differential drive spherical robot, as shown in Fig. 1(a).

A. Mechanical Design of the Spherical Robot

The proposed amphibious spherical robot aims to achieve flexible locomotion in both aquatic and terrestrial environments, particularly in confined spaces. As shown in Fig. 1(a), the robot features a three-module architecture: a central ring integrated with two symmetrically distributed paddle-wheel assemblies, forming a compact spherical configuration. This fully symmetric actuation system enables zero-radius steering capability, significantly enhancing maneuverability in spatially constrained scenarios. Fig. 1(b) details the modular design where the central ring houses the core electronic systems, including a Raspberry Pi controller, IMU sensor, wireless communication module, vision system with auxiliary lighting, and power supply. To ensure effective thermal management, the central ring employs lightweight aluminum alloy construction.

The hermetic sealing system employs multi-stage O-ring gaskets at the central ring-hemispherical shell interfaces, forming a pressure-resistant compartment with IP68 rated watertight integrity. This structural isolation ensures stable hydrodynamic performance during amphibious transitions. With a 255 mm spherical diameter and 2.6 kg total mass, the prototype maintains gravitational-buoyant equilibrium at 50% submersion depth. Two motors (J4310, DAMIAO, China), symmetrically mounted in the hemispherical compartments, deliver power through 1.5:1 reduction gear trains to the Halbach-array magnetic couplings. These advanced magnetic bearings (7 Nm torque capacity) drive the dual-purpose paddle-wheel assemblies. The innovative wheel-paddle hybrid end effector demonstrate multimodal functionality:

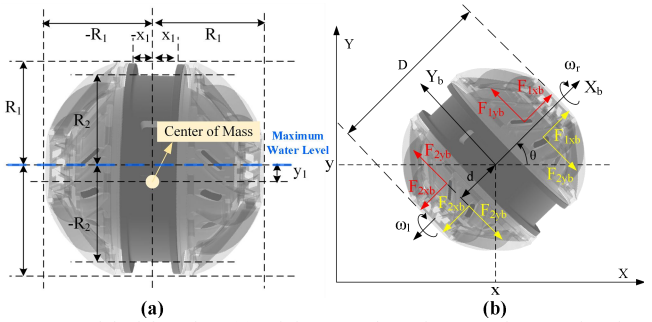

Fig. 2. Model of the robot. (a) Minimum and Maximum Volume Estimation of the Water dispersed by the Spherical Robot for calculation of the Buoyancy Force; (b) Simplified Schematics of the Dynamics of Hybrid Differential Drive Spherical Robot.

(1)Terrestrial mode: Ground contact surface enables differential steering via wheel rotation; (2) Aquatic mode: Arrayed paddle elements generate propulsive forces through hydrodynamic interaction.

B. Design for Floating over Water Surface

The use of paddle wheels requires the spherical robot to be half-immersed in water to prevent the neutralizing of the thrustforce by the returning stroke of the paddles. This shortcoming also gives forth two advantages: 1) the spherical robots can specifically be useful for monitoring and surveillance while swimming over the water surface; 2) half-immersion halves the motor torque and energy expenditure for aquatic motion. To ensure this floating motion, the weight of the robot should be balanced by the weight of the water displaced by its immersed volume, i.e. buoyancy force. However, for stability, the center of mass of the robot should remain immersed inside water. The maximum and the minimum height of the immersed volume of the robot are shown in Fig. 2(a).

The minimum volume of the water displaced by the spherical robot when it is immersed up to the height y_1 of its center of mass is given as:

$$V_{\min} = \int_{-R_2}^{-y_1}\int_{-R_2}^{-x_1} 2\sqrt{R_2^2 - y^2 - x^2}\,dxdy + \int_{-R_2}^{-y_1}\int_{R_2}^{x_1} 2\sqrt{R_2^2 - y^2 - x^2}\,dxdy + \int_{-R_1}^{-y_1}\int_{-x_1}^{x_1} 2\sqrt{R_1^2 - y^2 - x^2}\,dxdy \quad (1)$$

The corresponding minimum weight of the spherical robot can be written as:

$$W_{\min} = \rho_{water} V_{\min} \quad (2)$$

Similarly, if the spherical robot is immersed inside water up to its centroid, which is the maximum volume that should be immersed in water, then this volume is expressed by:

$$V_{\max} = \int_{-R_2}^{0}\int_{-R_2}^{-x_1} 2\sqrt{R_2^2 - y^2 - x^2}\,dxdy + \int_{-R_2}^{0}\int_{R_2}^{x_1} 2\sqrt{R_2^2 - y^2 - x^2}\,dxdy + \int_{-R_1}^{0}\int_{-x_1}^{x_1} 2\sqrt{R_1^2 - y^2 - x^2}\,dxdy \quad (3)$$

The maximum weight of the spherical robot is, therefore, given by:

$$W_{\max} = \rho_{water} V_{\max} \quad (4)$$

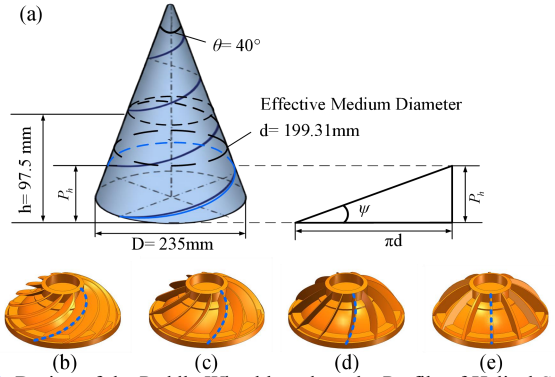

Fig. 3. Design of the Paddle Wheel based on the Profile of Helical Screw Thread. (a) The base ring diameter D, height h of the smallest ring of the Paddle Wheel, and the cone angle θ were fixed for all Paddle Wheel Designs. The diameter d_0 of the smaller end of the cone is determined based on the above-mentioned three fixed parameters. The effective medium diameter d is calculated by using $(d_0 + D)/2$; (b) Paddle Helix-1; (c) Paddle Helix-2; (d) Paddle Helix-3; (e) Straight Paddle.

TABLE I. PARAMETERS OF THE 4 PADDLE WHEELS

Item	Pitch P_h (mm)	Helix Angle ψ (°)
Paddle Helix-1	306.4	26
Paddle Helix-2	650	46
Paddle Helix-3	1410.5	66
Paddle Straight	Infinite	90

The range of weight of the spherical robot expressed by the above equations ensures enough immersion in water for stable aquatic motion and keeps the onboard cameras above the water surface.

C. Paddle Design

The holonomic linear motion of the spherical robot in water, its in-place turning, and arc-turning motion relies on its propeller to generate large forward and sideways forces. The spherical structure of the robot requires novel solutions for the robot's propulsion in water. For this, we explored the paddle-wheel structures in this paper. The paddle shapes were based on the helical screw thread, as shown in Fig. 3(a).

Four different paddle shapes were designed based on the combination of two variable parameters, pitch P_h and helix angle ψ, in addition to other fixed parameters. The relationship between the two parameters is given by:

$$\psi = \arctan\left(\frac{P_h}{\pi d}\right) \quad (5)$$

The design parameters of the four blades are given in Table I, and the paddle shapes are shown in Fig. 3(b), (c), (d) and (e).

C. Controller Design

The proposed spherical robot can be kinematically equivalent to a differential-drive configuration. However, the centralized placement of motors and batteries at the base positions the center of gravity below the wheel axle, forming a pendulum-like system. While this configuration provides inherent static stability, practical operation reveals that external disturbances or imbalanced actuation may induce periodic pitch oscillations, thereby compromising overall system stability.

Algorithm 1: Hierarchical Controller for the Amphibious Spherical Robot

Input: Desired wheel commands $(\omega_{r,cmd}, \omega_{l,cmd})$, reference pitch angle θ_{ref}
Sensors: IMU (pitch θ, angular velocity $\dot{\theta}$), wheel encoders (ω_r, ω_l)
Initialization: PID parameters for attitude loop, PI parameters for speed and current loops
While robot is operating **do**

1. Attitude compensation loop

$$e_\theta \leftarrow \theta_{ref} - \theta$$
$$\Delta\omega_p \leftarrow \mathrm{PID}_\theta(e_\theta, \dot{\theta})$$

2.Speed reference generation

$$\omega_r^* \leftarrow \omega_{r,cmd} + \Delta\omega_p$$
$$\omega_l^* \leftarrow \omega_{l,cmd} + \Delta\omega_p$$

3. Speed control loops

$$e_r \leftarrow \omega_r^* - \omega_r$$
$$e_l \leftarrow \omega_l^* - \omega_l$$
$$i_{q,r}^* \leftarrow \mathrm{PI}_\omega(e_r)$$
$$i_{q,l}^* \leftarrow \mathrm{PI}_\omega(e_l)$$

4.Current control loops

Apply $i_{q,r}^* \rightarrow$ MotorR
Apply $i_{q,l}^* \rightarrow$ MotorL

End While

To suppress pitch disturbances, we implement a hierarchical cascade control architecture consisting of three layers: current loop - velocity loop - attitude compensation loop (Fig. 1(c)). As the Algorithm 1, The bottom-level current loop ensures rapid linear response of motor torque. The intermediate velocity loop achieves precise tracking of bilateral wheel speeds. The top-layer attitude compensation loop employs PID control to generate corrective signals based on real-time pitch angle measurements from the IMU. These compensation terms are superimposed onto the reference wheel speeds through a common channel, enabling dynamic pitch stabilization without altering the fundamental differential steering mechanism. This architecture demonstrates robust adaptability for both terrestrial and aquatic environments while maintaining stability for onboard vision and communication systems.

III. Dynamics of the Spherical Robot on Water

The hybrid differential drive spherical robot employs the differential drive dynamics, which simplifies its dynamic analysis and motion control. Assuming there is no motion of the robot about its vertical z-axis, its motion can be reduced to planar motion, as shown in Fig. 2(b). There are three state variables of the robot, namely the linear displacement x along X-axis, linear displacement y along Y-axis, and the heading angle θ of the robot. The robot's motion in aquatic environment is based on the thrust force generated by its two propellers, which is controlled by controlling the angular velocity ω of the two propellers. The dynamics of the three motion modes of the robot are discussed in the following sub-sections. The viscous drag effects have been ignored in this dynamics section.

A. Holonomic Linear Motion of the Spherical Robot

A great advantage of the hybrid differential drive spherical robot is that it can be designed to be achieve a holonomy to a certain extent in aquatic environment by designing its propellers to generate forces along both its X_b and Y_b axes, as shown in Fig. 2(b). The direction of force components shown in red and yellow colors are based on the direction of rotation of the two propellers. If the heading angle of the robot is zero, i.e. $\theta = 0$, then $[X_b, Y_b] = [X, Y]$. Considering the same direction of rotation of the two propellers, and disregarding the signs of the F_y forces, the forces and moments acting on the robot are given by D'Alembert's principle as:

$$\begin{aligned} \sum F_x &= F_{1x} - F_{2x} \\ \sum F_y &= F_{1y} + F_{2y} \\ \sum M_z &= (F_{1y} - F_{2y})d \end{aligned} \tag{6}$$

It can be seen from (6), when both propellers generate equal forces in the same direction, the forces in the x-direction and the moments are canceled out. The robot in this case moves linearly forward or backward under the forces in y-axis direction, depending on the direction of rotation of the propellers. The planar accelerations of the robot can be expressed by Newton's second law as:

$$\begin{bmatrix} \ddot{x} & \ddot{y} & \ddot{\theta} \end{bmatrix}^T = \begin{bmatrix} 0 & \dfrac{\sum F_y}{m} & 0 \end{bmatrix}^T \tag{7}$$

In addition to forward and backward motion, linear motion of the robot is any other direction can be realized by carefully controlling the forces generated by the two propellers individually. This characteristic of the hybrid differential drive spherical robot makes the robot useful across diverse application scenario.

B. In-place Turning Motion of the Spherical Robot

For the in-place turning motion of the hybrid differential drive spherical robot in water, its two propellers must generate equal and opposite forces along the Y-axis direction. In such a case, using the D'Alembert's principle:

$$\begin{aligned} \sum F_x &= F_{1x} - F_{2x} = 0 \\ \sum F_y &= F_{1y} - F_{2y} = 0 \\ \sum M_z &= (F_{1y} + F_{2y})d \end{aligned} \tag{8}$$

In (8), it can be seen that the forces of the two propellers along the X and Y axes are canceled out. However, the moments generated by the F_{1y} and F_{2y} generates couple, which leads to the in-place turning motion of the spherical robot. In the above equation, d is the perpendicular distance between the robot's centroid and the line of action of force F_{1y} or F_{2y}. If I is the moment of inertial of the robot, then the planar accelerations of the spherical robot in such a scenario can be expressed as:

$$\begin{bmatrix} \ddot{x} & \ddot{y} & \ddot{\theta} \end{bmatrix}^T = \begin{bmatrix} 0 & 0 & \dfrac{\sum M_z}{I} \end{bmatrix}^T \tag{9}$$

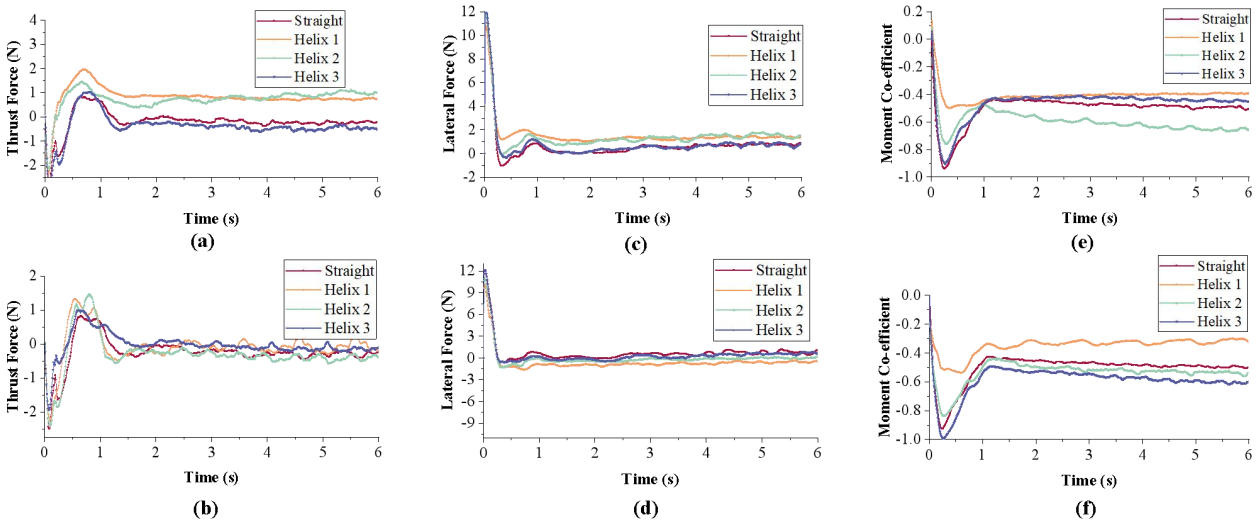

Fig. 4. Hydrodynamic Analysis and Design Optimization of the four Paddle Wheel Designs through Computational Fluid Dynamic (CFD) Simulations. (a), (c), and (e) show the Thrust Force, Sideways Lateral Force, and the Moment Coefficient during Forward Motion, respectively; (b), (d), and (f) show the Thrust Force, Sideways Lateral Force, and the Moment Coefficient during Backward Motion, respectively.

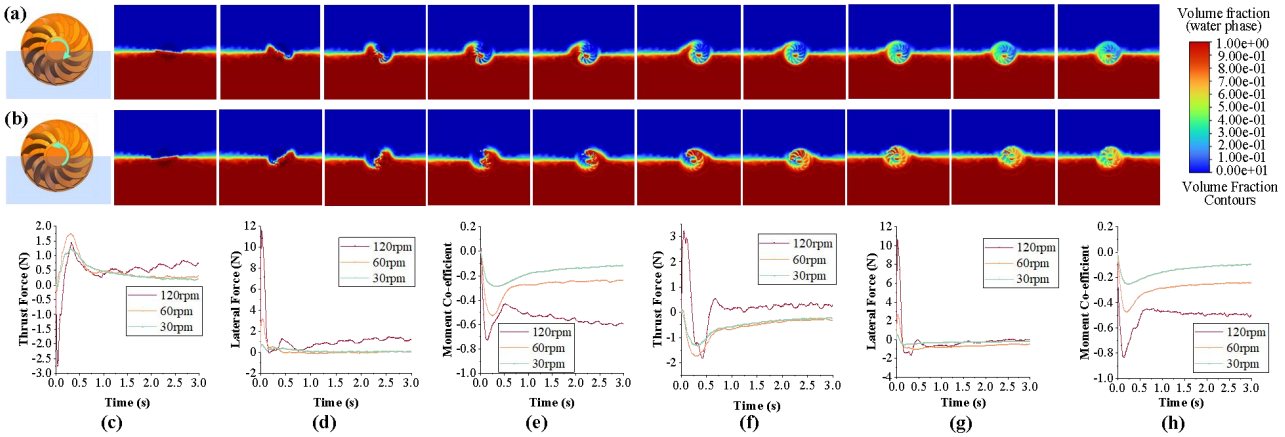

Fig. 5. Transient-state CFD Simulation Results of the Helix-2 Paddle Wheel Design over the Surface of Water. (a) Volume Fraction Contours during Forward Motion of Helix-2 Wheel at 120rpm; (b) Volume Fraction Contours during Backward Motion of Helix-2 Wheel at 120rpm; (c), (d), and (e) show the Thrust Force, Sideways Lateral Force, and the Moment Coefficient at three different angular speeds of Helix-2 Wheel during Forward Motion, respectively; (f), (g), and (h) show the Thrust Force, Sideways Lateral Force, and the Moment Coefficient at three different angular speeds of Helix-2 Wheel during Backward Motion, respectively.

C. Arc-Turning Motion of the Spherical Robot

To reach any desired planar location, the combination of the linear and in-place turning motion can be used. However, this strategy is not efficient and requires frequent switching of motion modes. Therefore, it is necessary for any mobile robot to be capable of arc-turning motion. To realize this, the twopropellers of the hybrid differential drive spherical robot must generate forces F_y in the same direction but with different moments acting on the robot are given as:

$$\begin{aligned} \sum F_x &= F_{1xb}\cos\theta - F_{2xb}\cos\theta - F_{1yb}\sin\theta - F_{2yb}\sin\theta \\ \sum F_y &= F_{1xb}\sin\theta - F_{2xb}\sin\theta + F_{1yb}\cos\theta + F_{2yb}\cos\theta \\ \sum M_z &= (F_{1yb} + F_{2yb})d \end{aligned} \tag{10}$$

In (10), the subscript *b* represents the body frame of reference. It can be seen that unlike other modes of the motion, the arc-turning motion of the hybrid differential drive spherical robot requires careful control of all the forces. Moreover, due to the presence of unequal forces along the X_b-axis, there will be sideways skidding motion as the robot turns along an arc.

The planar accelerations of the robot during arc-turning motion can be expressed as:

$$\begin{bmatrix} \ddot{x} & \ddot{y} & \ddot{\theta} \end{bmatrix}^T = \begin{bmatrix} \dfrac{\sum F_x}{m} & \dfrac{\sum F_y}{m} & \dfrac{\sum M_z}{I} \end{bmatrix}^T \tag{11}$$

It can be observed from (6), that by the precise control of the forces of the two propellers, the turning motion of the spherical robot can be realized with different turning radii.

IV. Computational Fluid Dynamic (CFD) Simulations

To analyze the hydrodynamic performance of the designed paddle wheels, we performed CFD simulations. The simulation results provide a strong basis for optimizing design parameters. Therefore, CFD analysis represents a critical part of this study.

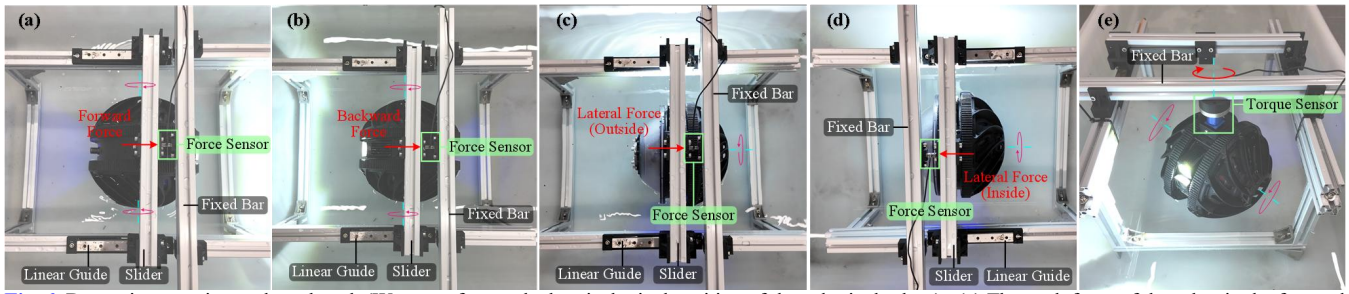

Fig. 6. Dynamics experimental test bench (Water surface at the hemispherical position of the spherical robot). (a) The push force of the robot in the forward direction; (b) The push force of the robot in the backward direction; (c) The lateral force of the robot in the outside direction (paddle wheel rotate in forward direction); (d) The lateral force of the robot in the inside direction (paddle wheel rotate in backward direction); (e) The torque of turning action.

A. Simulation Setup

The hydrodynamic performance analysis for the design parameter optimization was carried out through CFD simulations in Ansys Fluent. As the paddle wheel rotates over the surface of the water, half immersed in water and half in air, this simulation scenario is a transient, multiphase, turbulent flow problem with mesh rotation. This makes the simulation computationally expensive. Therefore, efforts were made to decrease the computational time without costing the solution accuracy and stability. For this specific simulation scenario, Volume of Fluid (VOF) multiphase model is best suited, which does not support GPU-based acceleration. The fluid domain was kept large enough so that the reverse flow does not influence the thrust force. The total number of mesh elements were just above 300,000, with the elements size ranging from 6x10e-06 to 3x10e-03. The simulations assume large swimming pool with zero Reynolds number. SIMPLE pressure-velocity coupling scheme was used, which decreased the computational time by ten times, at least over different simulation cases. For Volume Fraction, Modified HRIC discretization was selected. The options, such as high order term relaxation were de-selected for efficiency. Implicit volume fraction parameter formulation was used, which is stable for relatively large CFL numbers. Since the flow velocity near the paddle tips are larger and the mesh element size is kept lower in that region to capture the physics, a low fixed time-step size of 0.005 was selected for the solution stability. Using this simulation setup, a single case of simulation of 7 seconds physical time is completed in 8hours using 4 cores parallel processing on a desktop computer with i7-14700KF CPU and 32GB RAM with 6400MHz frequency.

B. Comparison of Hydrodynamic Performance of Paddle Wheel Designs

The four paddle wheel profiles, shown in Fig. 3, were first analyzed through CFD simulations. The simulation results of each wheel are compared in Fig. 4. It can be seen in Fig. 4(a) and 4(b) that the thrust force increases with the decrease in helix angle for both forward (positive value is better) and backward (negative value is better) rotation. Helix-2 design performs the best in terms of thrust force generation. However, the results for the sideways force are mixed. The Helix-2 design generates largest sideways force during forward rotation, but it performs worst in sideways force generation during backward rotation. The Helix-1 represents the best design for sideways force generation. The moment coefficient results represent how much motor torque is required to rotate the paddle wheel in the given scenario (positive is better). It can be seen that the Helix-1 designs is the most energy efficient design, whereas Helix-2 requires large motor torque. However, the forward and backward thrust generation and the sideways force generation determines the agile motion of the spherical robot in water. Therefore, Helix-2 design represents the best among the four designs.

To further evaluate the hydrodynamic performance and analyze its thrust generation, we ran more simulations for the Helix-2 design at three different rotation speeds (30rpm, 60rpm, and 120rpm) in both forward and backward directions. The results for the forward rotation are shown in Fig. 5. In Fig. 5(c), it can be seen that the paddle wheel generates large forward thrust force (positive is better) and later force at 120rpm, which is exponentially larger than those at 30rpm and 60 rpm. Similarly, plots in Fig. 5(f) shows larger backward thrust force (negative is better) at 120rpm. However, the backward thrust is much lower as compared to the forward thrust. Moreover, the lateral force is insignificant for the backward motion.

The water volume fraction contours are shown in Fig. 5(a) and Fig. 5(b) during the initial stages of the paddle's rotation. As the paddle begins to rotate, the surface tension applies force against the concave surface of the paddle during forward motion, thus exerting a large backward force initially. However, the convex surface of the paddle helps in the backward motion and thus a large negative thrust is generated. However, over long interval, the convex shape experiences larger drag force, thus reducing the thrust force. It can also be seen, as expected, the larger the rotation speed of paddle wheel, the larger is the moment coefficient.

V. Experiments And Results

In this paper, we focus on evaluating the feasibility and effectiveness of the proposed paddle-wheel (the parameters in Table I, the Helix-2) for the spherical robot. As shown in Fig.6, a modular experimental testbed was constructed to evaluate robotic thrust performance. Subfigures 6(a) through 6(d) incorporate force sensor (DYLY-107, Dayang, China) for precise force measurement: specifically, Fig.6(a) measures forward thrust of the paddle-wheel configuration, Fig.6(b) evaluates reverse thrust characteristics, while Figs.6(c) and 6(d) assess lateral thrust in outward and inward directions respectively. To address differential torque measurement requirements, the setup in Fig.6(e) employs a dedicated torque sensor (DYJN-107, Dayang, China) for comprehensive evaluation of torsional dynamics. As the robot propels in the water, it will move forward or backward along with the slider,

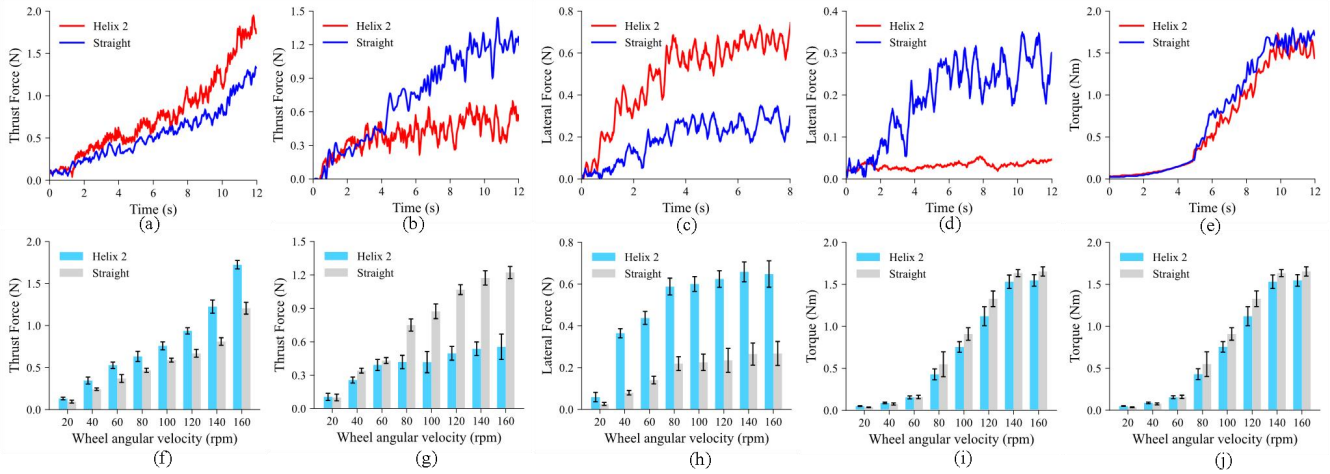

Fig. 7. Bench test of the selected paddle (Helix-2) with the straight paddle. (a) Data of the push force of the robot in the forward direction; (b) Data of the push force of the robot in the backward direction; (c) Data of the lateral force of the robot in the outside direction (paddle wheel rotate in forward direction); (d) Data of the lateral force of the robot in the inside direction (paddle wheel rotate in backward direction); (e) The torque of turning action; (f) Statistical result of forward force in different speeds; (g) Statistical result of backward force in different speeds; (h) Statistical result of lateral force (outside) in different speed; (i) Statistical result of lateral force (inside) in different speed; (j) Statistical result of torque in different speed.

TABLE II. RESULTS BETWEEN THE HELIX 2 AND STRAIGHT PADDLE WHEELS IN FORWARD DIRECTION

Wheel speed (rpm)	Thrust Force (N)		Improvement	Lateral Force (N)		Improvement
	Helix-2	Straight	(%)	Helix 2	Straight	(%)
20	0.131±0.015	0.094±0.017	39.36	0.059±0.023	0.026±0.007	126.92
40	0.345±0.042	0.243±0.015	41.98	0.365±0.022	0.080±0.011	356.25
60	0.527±0.038	0.370±0.046	42.43	0.438±0.031	0.141±0.018	210.64
80	0.632±0.061	0.468±0.025	35.04	0.588±0.040	0.219±0.033	168.49
100	0.759±0.048	0.588±0.023	29.08	0.600±0.036	0.226±0.039	165.49
120	0.936±0.038	0.669±0.047	39.91	0.624±0.040	0.235±0.057	165.53
140	1.224±0.078	0.810±0.045	51.11	0.648±0.047	0.265±0.053	144.53
160	1.724±0.050	1.207±0.071	42.83	0.658±0.063	0.268±0.057	145.52

thus hitting the force sensor, which measures the push force exerted on it and thus the agility of the robot. For measuring the thrust force, the paddle is rotated in both forward and backward direction. For measuring the lateral force, only one of the paddle wheels is used.

The spherical equatorial plane was maintained at water level. The impeller speed was uniformly accelerated from 0 to 160 rpm over 12s to investigate hydrodynamic characteristics under different operational modes. Comparative experiments were conducted between straight-bladed and helical-bladed impellers, evaluating five typical motion patterns: forward, backward, lateral force (outside), lateral force (inside), and in-situ turning.

Forward Thrust: As depicted in Fig. 7(a), both propeller configurations exhibited approximately linear thrust growth with increasing rotational speed. The helical blade consistently generated higher thrust throughout the test, achieving a maximum of 2.0 N compared to 1.5 N for the straight blade (30% enhancement). This superiority arises from the helical blade's continuous fluid-structure interaction enabled by its spiral lead angle, which reduces thrust pulsations, drag, and simultaneously applies tangential and axial forces to optimize momentum transfer efficiency.

Backward Thrust: Fig. 7(b) demonstrates backward performance characteristics during backward propulsion. The straight blade achieved a maximum reverse thrust of 1.2 N, significantly outperforming the helical blade's 0.7 N. This discrepancy stems from the directional optimization of helical blades for forward operation. During reverse rotation, unfavorable water-entry angles increase flow disturbances and reduce effective propulsion area, while the straight blade's structural symmetry maintains consistent hydrodynamic action in both directions.

Lateral Force Outside: Under unilateral operation (Fig. 7(c)), the helical blade generated 0.8 N lateral force at 160 rpm, exceeding the straight blade's 0.3 N. This enhancement originates from the helical blade's ability to induce strong tangential flow components during rotation, creating amplified lateral momentum transfer. While beneficial for holonomy if controlled precisely, this mechanism introduces lateral disturbances requiring compensation.

Lateral Force Inside: In rotation tests (Fig. 7(d)), the straight blade maintained superior lateral force output (0.3 N) compared to the helical blade's limited 0.05-0.1 N range. The helical blade's reverse operation induces severe flow separation due to geometric incompatibility, whereas the straight blade's bidirectional symmetry ensures stable reverse flow interaction and robust lateral thrust generation.

In-situ Torque: Both propellers produced stable spinning torque (1.8-2.0 Nm) during counter-rotating operation (Fig. 7(e)). The straight blade showed slightly higher torque during

mid-stage acceleration (6-10 s), while the helical blade demonstrated smoother operation at high speeds with reduced fluctuations. This behavior reflects fundamental design differences: the straight blade's geometric simplicity enables direct transient response, whereas the helical blade forms continuous flow channels for stabilized high-speed performance.

The helical blade demonstrates 30% forward thrust improvement and 167% lateral force superiority in operation, confirming its hydrodynamic advantages through optimized spiral-induced flow control. Its smoother torque delivery during spinning further validates energy transfer efficiency. Although the straight blade exhibits reverse operation superiority (41% higher thrust) due to structural symmetry, the helical blade's comprehensive performance in primary motion modes (forward propulsion, lateral maneuvering, and spinning stability) significantly enhances the spherical robot's aquatic mobility and operational precision.

The experimental (Table. II) results clearly demonstrate the helical blade's superior performance in both forward thrust and lateral force generation during unilateral CW rotation compared to the straight blade. Specifically, for forward thrust, the helical blade maintains a consistent enhancement range of 30%-50% across all rotational speeds, with a peak improvement of 51.11% at 140 rpm. This indicates its higher energy conversion efficiency and stable performance advantages during forward propulsion. In lateral force generation, the helical blade exhibits even more pronounced superiority. At low-speed ranges (20-40 rpm), its improvement magnitude reaches 126.92%-356.25%, while retaining significant enhancements of 145%-166% at high-speed ranges (100-160 rpm). These results confirm the helical blade's capability to generate stronger lateral forces during unilateral actuation, thereby substantially improving the spherical robot's surface maneuverability and steering responsiveness. Collectively, the helical blade demonstrates not only sustained advantages in forward propulsion efficiency but also exceptionally significant improvements in lateral motion control capabilities.

VI. Conclusion

This study presented an amphibious spherical robot that integrates the structural symmetry of a sphere with the simplicity of differential-drive kinematics. Through mechanical design, buoyancy analysis, and hierarchical control, the robot demonstrated stable locomotion on both land and water. Comparative evaluation of four paddle-wheel configurations showed that the Helix-2 blade achieves the best overall balance of thrust, lateral maneuverability, and torque requirements. Both CFD simulations and experiments confirmed its performance, with forward thrust improved by up to 51% and lateral force enhanced by more than 160% compared with straight blade, thereby significantly strengthening aquatic mobility. Although reverse motion remains less efficient, the overall results establish the Helix-2 design as an effective solution for enhancing propulsion efficiency and maneuverability. Future efforts will focus on improving bidirectional propulsion and extending operational capability to long-duration aquatic tasks. Moreover, an in-depth parametric analysis of the blades design and experimental comparison in open waters remains a priority. Collectively, the findings confirm the feasibility of the hybrid differential-drive spherical robot as a practical platform for agile amphibious locomotion in complex environments.

VII. Video Attachments

This paper has a supplementary multimedia material, please refer to www.youtube.com/watch?v=0X2Q12ZkTlo for the detail.

References

[1] Diouf, A., et al., Spherical rolling robots—Design, modeling, and control: A systematic literature review. Robotics and Autonomous Systems, 2024. 175: p. 104657.

[2] Arif, M.A., et al., Design of an Amphibious Spherical Robot Driven by Twin Eccentric Pendulums With Flywheel-Based Inertial Stabilization. IEEE/ASME Transactions on Mechatronics, 2023. 28(5): p. 2690–2702.

[3] Melchiorre, M., et al. Design of a Spherical Rover Driven by Pendulum and Control Moment Gyroscope for Planetary Exploration. Robotics, 2024. 13, DOI: 10.3390/robotics13060087.

[4] Ren, W., et al., Spherical robot: A novel robot for exploration in harsh unknown environments. IET Cyber-Systems and Robotics, 2023. 5(4): p. e12099.

[5] Liu, Y., et al., Multi-Terrain Velocity Control of the Spherical Robot by Online Obtaining the Uncertainties in the Dynamics. IEEE Robotics and Automation Letters, 2022. 7(2): p. 2732–2739.

[6] Arif, M.A., et al. Design Roadmap for Non-Holonomic Spherical Robots Driven by Two Pendulums. in 2023 International Conference on Design Science (ICDS). 2023.

[7] Artusi, M., et al., Electroactive Elastomeric Actuators for the Implementation of a Deformable Spherical Rover. IEEE/ASME Transactions on Mechatronics, 2011. 16(1): p. 50–57.

[8] Zhang, Y., et al., Design and Implementation of a Deformable Spherical Robot With Rolling and Jumping Capabilities. IEEE Robotics and Automation Letters, 2025. 10(11): p. 11650–11657.

[9] Jangale, R. V., et al., Design of Soft Outer Shells for Control of Large Spherical Robots. IEEE Robotics and Automation Letters, 2025. 10(11): p. 11864–11871.

[10] Mukherjee, R., et al., Pukrushpan. Simple motion planning strategies for spherobot: a spherical mobile robot. in Proceedings of the 38th IEEE Conference on Decision and Control (Cat. No.99CH36304). 1999.

[11] Bu, S., et al., Design and Motion Control of Spherical Robot With Built-In Four-Wheel Omnidirectional Mobile Platform. IEEE Transactions on Instrumentation and Measurement, 2023. 72: p. 1–10. Art no. 7502910.

[12] Tafrishi, S.A., et al., Design, Modeling, and Motion Analysis of a Novel Fluid Actuated Spherical Rolling Robot. Journal of Mechanisms and Robotics, 2019. 11(4).

[13] Belzile, B. and D. St-Onge, ARIES: Cylindrical Pendulum Actuated Explorer Sphere. IEEE/ASME Transactions on Mechatronics, 2022. 27(4): p. 2142–2150.

[14] Asiri, S., et al., The Design and Development of a Dynamic Model of a Low-Power Consumption, Two-Pendulum Spherical Robot. IEEE/ASME Transactions on Mechatronics, 2019. 24(5): p. 2406–2415.

[15] Krieger, K., Meet the Guardbot. 2013.

[16] Arif, M.A., et al., Panoramic visual system for spherical mobile robots. Robotica, 2024. 42(7): p. 2089–2107.

[17] Xing, H., et al., Design, modeling and control of a miniature bio-inspired amphibious spherical robot. Mechatronics, 2021. 77: p. 102574.